ACS OMEGA

http://pubs.acs.org/journal/acsodf

Article

Influence of Nanopore Structure Deformation on Gas Migration in Coal

Xiaofeng Ji,* Dangyu Song, Wenfang Shi, and Yanfei Li

Cite This: *ACS Omega* 2021, 6, 19115−19126

Read Online

ACCESS | Metrics & More | Article Recommendations

ABSTRACT: To better understand the influence and control of nanopore characteristics on gas migration, three kinds of coal samples with different metamorphic degrees were selected for the experiments including high-pressure isothermal gas adsorption, low-pressure CO_2 adsorption, and low-pressure Ar adsorption. The changes of the pore volume (PV) and specific surface area (SSA) of coal samples before and after adsorption−desorption were compared and analyzed. The adsorption data of all coal samples at a low pressure stage (<8 MPa) conformed to the Langmuir equation, and the adsorption capacity of powdered coal samples was higher than that of columnar coal samples. Some adsorption data deviated from the original fitting curve at a high pressure stage (>8 MPa), and this was the most remarkable in columnar coal samples. There was a positive correlation between the cumulative SSA of pores and adsorption capacity of coal samples. When the adsorption time was more than 10 min, the adsorption efficiency of 200 mesh coal samples from YJL was lower than those of 200 mesh coal samples from CZ and WY, which was due to the good development and connectivity of micro-fissures and nanopores in YJL coal samples. The pore size distribution of coal samples had changed after adsorption−desorption, and the cumulative deformation of the nanopore structure was anisotropic. As a result of the swelling or shrinkage deformation of the coal matrix, the PV and SSA with the same pore size presented many forms, such as almost unchanged, increased, or decreased. There are two types of deformation mechanisms: the whole collaborative deformation and partial deformation. Both gas adsorption and desorption can lead to the shrinkage or swell deformation of nanopores and fissures. In brief, the research provides theoretical and technical support for reservoir evaluation, fine drainage, and efficient development of coalbed methane.

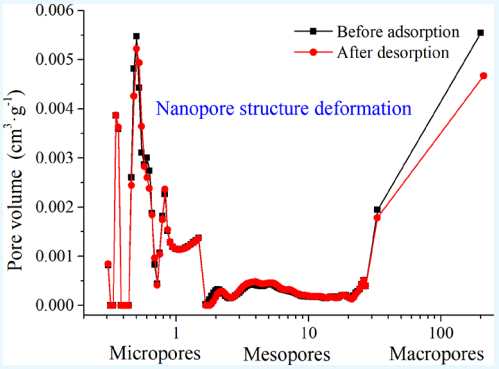

1. INTRODUCTION

There are complex fissure and pore systems in the coal reservoir, including multiscales from nanometer to centimeter, which is also an effective space for gas occurrence and migration.[1] The form and scale of gas migration in pores with different scales and shapes vary considerably. Even if the pores are the same scale, gas migration characteristics are different under different temperature and pressure conditions.[2] The International Union of Pure and Applied Chemistry (IUPAC) divided the pores into micropores (pore diameter <2 nm), mesopores (2−50 nm), and macropores (>50 nm) according to the size.[3] Generally, pores with a diameter of less than 100 nm are called nanopores. Previous researches showed that coalbed methane (CBM) generally occurred in nanopores, especially on the surface of micropores in the coal matrix.[4,5] There are three types of test methods for pore characteristics in coal: fluid injection, image analysis, and physical detection, as shown in Figure 1.

Fluid injection methods include mercury intrusion porosimetry (MIP), low-pressure CO_2 adsorption (LP-CA), low-pressure N_2 adsorption (LP-NA), and low-pressure Ar adsorption (LP-AA).[6,7] Image analysis methods include optical

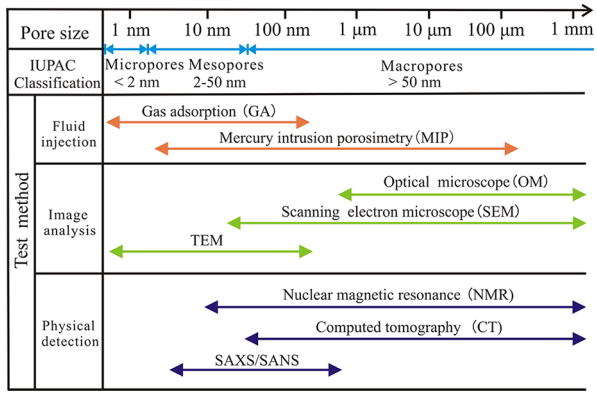

Figure 1. Test methods for pore characteristics.

Received: May 9, 2021
Accepted: June 29, 2021
Published: July 14, 2021

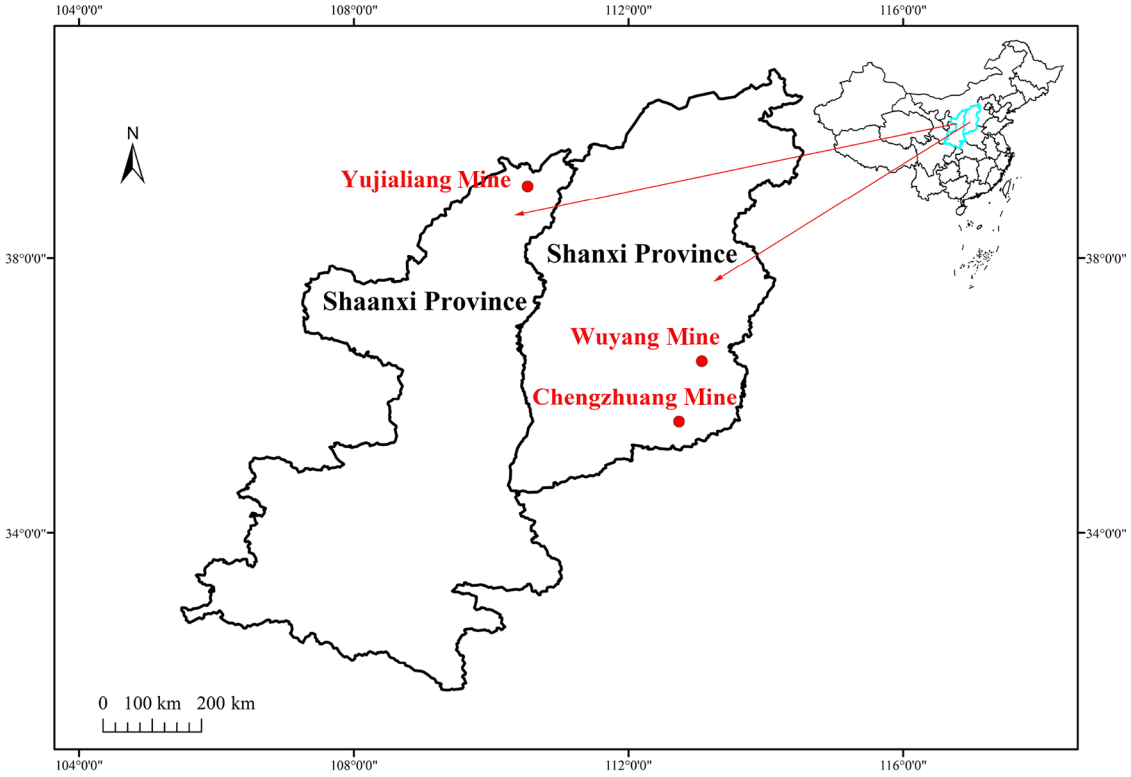

Figure 2. Location of coal sample collection.

microscopy (OM), scanning electron microscopy (SEM), and transmission electron microscopy (TEM).[8,9] Physical detection methods consist of nuclear magnetic resonance (NMR), computed tomography (CT), small-angle X-ray scattering (SAXS), and small-angle neutron scattering (SANS).[10−12]

However, due to the diversity in theoretical models and material characteristics, each test method only detects pores with a specific range.[13] High-pressure MIP can be used to analyze the structural information of open pores between 3 nm and 400 μm. However, the sample internal matrix tends to be compressed at a high level of injection pressure, thus resulting in unreliable analytical results of some nanopores.[14,15] LP-AA with the Barrett−Joyner−Halenda (BJH) model is suitable for analyzing the pore characteristics between 1.5 and 230 nm, while LP-CA with the non-local density functional theory (NLDFT) model is only applicable to analyze the pore characteristics less than 1.5 nm.[5] Compared with N_2, there is no interaction between Ar and the functional groups on the pores surface of coal, so LP-AA is recommended by the IUPAC for analyzing pore characteristics in coal.[3] Image analysis is an effective method for intuitively observing the partial characteristics but cannot quantitatively characterize the whole pore characteristics of samples. Nano-CT combined with the quartet structure generation set (QSGS) method can reconstruct the three-dimensional nanopore structure larger than 30 nm in coal.[16] To overcome these limitations and deficiencies, the combination of various test methods is a viable way to characterize the pore characteristics in coal.

The scale of gas adsorption and migration in the coal reservoir is related to material composition, distribution characteristics of pores and fissures, water content, reservoir temperature and pressure, and gas type.[17−20] The nanopore structure in coal is related to the coal rank and deformation structure. The proportion of transitional pores (10−100 nm) is the largest in pore volume (PV), and the proportion of submicropores (1.5−5 nm) is the largest in specific surface area (SSA).[21] The test results of isothermal adsorption and the pore structure show that the gas adsorption capacity of middle-high rank coal is mainly related to the SSA of micropores.[22] The particle size of coal samples also affects the measurement results of the pore structure, the adsorption equilibrium time is related to the distribution characteristics and connectivity of pores with different scales, and it takes a longer time to enter smaller pores.[23] Based on deformable organic carbon slit pore models, the absorption of carbon dioxide is simulated by the Grand Canonical Monte Carlo (GCMC) method, and it is found that both swelling deformation and shrinkage deformation are sensitive to the pore size.[24] The deformation of adsorbed gas in the coal matrix contributes to the change of the PV and porosity in coal and eventually affects the change of permeability.[25,26] For dry coal samples, the adsorption capacity of coal decreases with the increase in particle size.[27,28] Most of previous studies focused on the relationship between gas adsorption and pore distribution and ignored the influence of the deformation of different types of nanopores on the migration speed and scale of CBM.

In this study, different metamorphic coal samples were selected as the research object and the isothermal adsorption experiments of coal samples with different particle sizes (200 mesh, 60−80 mesh, and columnar) were performed. Based on the original data of pressure and time, the adsorption capacity at different times was analyzed and calculated. Meanwhile, the intrinsic relationship between the adsorption behavior and nanopores was analyzed. Using the LP-CA and LA-AA method, the pore structure of 60−80 mesh coal samples before and after adsorption−desorption was measured and analyzed. In addition, the deformation characteristics of different types of nanopores were analyzed and the influence

https://doi.org/10.1021/acsomega.1c02442
ACS Omega 2021, 6, 19115−19126

mechanism of pore structure differences and deformation on gas occurrence or migration was explored.

2. MATERIALS AND METHODS

2.1. Sample Collection. The selection of coal samples should consider the differences of metamorphic degree, gas production capacity and permeability, and specific representativeness. The coal samples were collected from the Yujialiang Mine in the Shenmu mining area, Wuyang Mine in the Luan mining area, and Chengzhuang Mine in the Jincheng mining area. All these mines are hot areas of CBM development and research in China, and their geographical location is shown in Figure 2. The sampling sites are all located in the coal mining face or heading face, with a size of 30 cm × 30 cm × 30 cm.

2.2. Preparation of Coal Samples of Different Sizes. The collected fresh coal samples were drilled into columnar samples with a diameter of 25 mm and a height of 50 mm. To ensure the similarity of the composition of coal samples with different particle sizes, the raw coal from same layers was crushed into 60−80 mesh powdered samples for pore structure testing and 200 mesh powdered samples for proximate analysis. Both columnar and powdered coal samples were used in the high-pressure isothermal methane adsorption (HP-CH_4GA) experiments. To eliminate the influence of moisture on gas adsorption, all the coal samples were placed in a drying oven at 70 °C for more than 48 h until the weight discrepancy was less than 0.01 g.

2.3. Experiments. *2.3.1. Proximate Analysis and Vitrinite Reflectance.* According to the national standard (GB/T 30732-2014, 2014),[29] an automatic proximate analyzer (5E-MAG6700, Changsha Kaiyuan Instrument Co., Ltd., China) was used for proximate analysis.

Vitrinite reflectance ($R_{o,max}$) determination was performed with a polarizing microscope and spectrophotometer (Axioskop-40, ZEISS, Germany), according to the national standard (GB/T 6948-2008, 2008).[30]

2.3.2. HP-CH_4GA Experiments. Depending on the national standard (GB/T 19560-2008, 2008),[31] the HP-CH_4GA experiments were conducted using a volumetric-based adsorption−desorption instrument (ISO-300, TerraTek, USA).

The experimental facilities mainly included a temperature and pressure control system, adsorption and desorption system, data acquisition and control system, vacuum degassing device, matching pipeline, and sensors. The maximum experimental pressure was 34.5 MPa, the maximum experimental temperature was 100 °C, and the temperature control stability was ±0.5 °C. The experimental process included sample loading, air tightness inspection, free space volume measurement, setting experimental conditions, isothermal adsorption−desorption experiment, data collection, and result analysis. Seven target pressure points (1, 2, 4, 6, 8, 10, and 12 MPa) were set in the isothermal adsorption experiments. The experimental temperature was set at 30 °C. According to the national standard (GB/T 19560-2008, 2008),[29] the adsorption equilibrium time of powdered coal samples was not less than 12 h. Therefore, for powdered coal samples of 60−80 and 200 mesh, the adsorption equilibrium time was set to 12 h. For columnar coal samples, the adsorption balance time was set to 36 h.

The software of the instrument can automatically record the pressure data at different times. According to the calculation principle of the volume method, the adsorption capacity of coal samples under different time and equilibrium conditions can be obtained.[32]

2.3.3. Low-Pressure Gas Adsorption Experiments. An Autosorb-IQ porosity and surface area analyzer (Autosorb IQ-MP, Quantachrome Instruments, USA) were used to conduct low-pressure gas adsorption tests on the basis of the national standards (GB/T 21650.2-2008, 2008; GB/T 21650.3-2011, 2011).[33,34] The adsorbates used in low-pressure gas adsorption experiments include CO_2, N_2, and Ar. The corresponding experimental temperatures were 273, 77, and 87 K, respectively, which were related to their boiling points. Based on some adsorption theories, different analytical models were used to analyze the parameters of the nanopore structure in coal, including the SSA and PV. The application scope of different calculation models for coal nanopore characteristic analysis is shown in Table 1.

Table 1. Analysis of Nanopore Characteristics with Different Calculation Models[a]

adsorbate	calculation model	pore size (nm)	test items
CO_2	NLDFT	0.3−1.5	PV, SSA, PSD
	MC	0.3−1.5	PV, SSA, PSD
	DA	0.02−6	PV
N_2/Ar	BJH	1.5−230	PV, SSA, PSD
	QSDFT	0.35−30	PV, SSA, PSD
	NLDFT	0.35−40	PV, SSA, PSD
	BET	1.5−230	SSA

[a]Note: PV, pore volume; SSA, specific surface area; PSD, pore size distribution.

To reduce the analysis error, the IUPAC proposed using Ar to analyze the nanopore characteristics in coal.[3] Therefore, CO_2 and Ar were used as adsorbates in this study.

3. RESULTS AND DISCUSSION

3.1. Coal Quality Analysis and Coal Rank. The proximate analysis and vitrinite reflectance results of coal samples are shown in Table 2.

The coal samples include anthracite, low volatile bituminous coal, and high volatile bituminous coal, with maximum vitrinite reflectances of 3.01, 2.06, and 0.65%, respectively.

3.2. Influence of Nanopore Characteristics on Gas Adsorption and Migration. *3.2.1. Influence of Particle Size on Adsorption Characteristics.* The isotherm adsorption curve can be used to analyze the physical parameters of the CBM reservoir and evaluate the storage and production capacity of CBM. According to the experimental principle and the original data, the corresponding gas adsorption date under different equilibrium pressures was calculated and these data were modified by dry ash-free basis. Combined with the Langmuir adsorption theory,[35] the isothermal adsorption curves of coal samples are fitted by the Langmuir equation, as shown in Figure 3.

From Figure 3, when the gas pressure is lower than 8 MPa, all adsorption data of coal samples are highly fitted with the Langmuir equation and the adsorption data is almost on the fitting curves. When the gas pressure is higher than 8 MPa, some adsorption data deviates from the original fitting curves, and this is more obvious in columnar coal samples. In the high-pressure stage, the original fissures or micro-fissures in columnar coal samples are easy to be widened or extended, thus forming a new migration channel and occurrence space

https://doi.org/10.1021/acsomega.1c02442
ACS Omega 2021, 6, 19115−19126

Table 2. Proximate Analysis and Vitrinite Reflectance Results[a]

sample number	location	proximate analysis			$R_{o,max}$ (%)	coal rank
		M_{ad} (%)	A_{ad} (%)	V_{daf} (%)		
CZ	Chengzhuang Mine, Shanxi Province	2.56	9.62	7.74	3.01	anthracite
WY	Wuyang Mine, Shanxi Province	1.00	8.83	13.20	2.06	bituminous coal
YJL	Yujialiang Mine, Shaanxi Province	6.17	3.54	29.51	0.65	bituminous coal

[a]Note: M_{ad}, moisture content on an air-dry basis; A_{ad}, ash content on an air-dry basis; V_{daf}, volatile content on a dry, ash-free basis; $R_{o,max}$, maximum vitrinite reflectance under oil immersion.

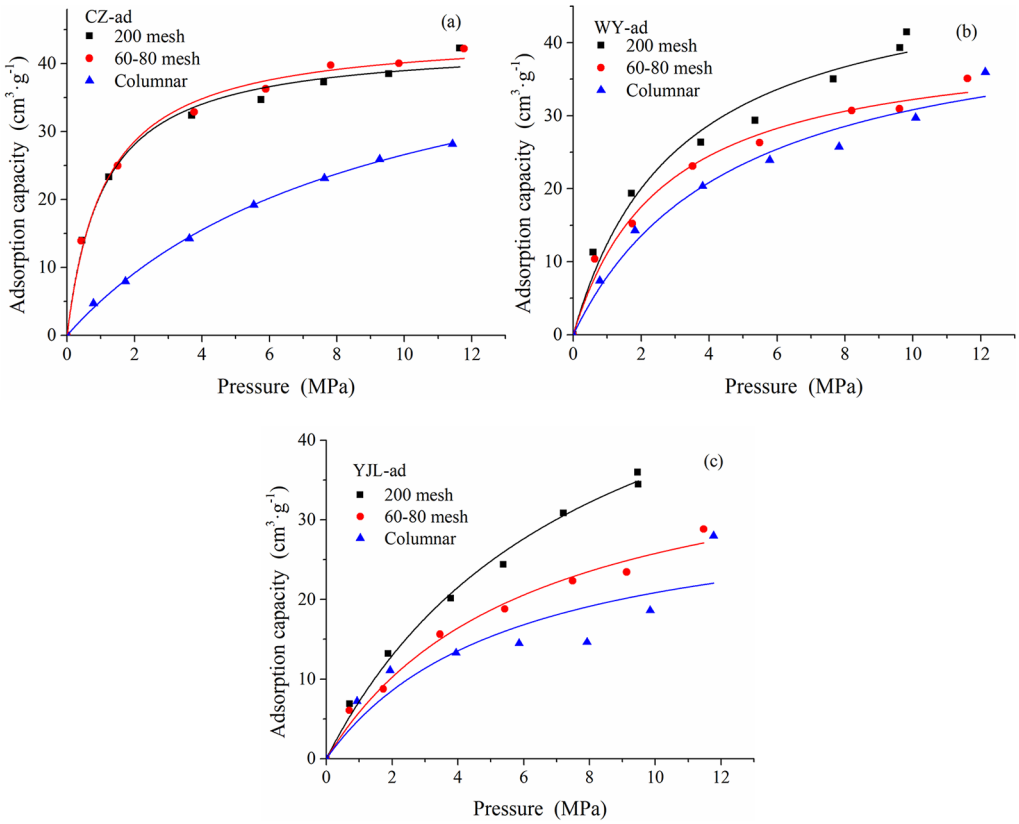

Figure 3. Isothermal adsorption curves of coal samples. (a) Three kinds of coal samples from CZ. (b) Three kinds of coal samples from WY. (c) Three kinds of coal samples from YJL.

and resulting in a sudden increase in adsorption capacity. By comparison, the powdered coal samples contained fewer fissures and micro-fissures and the increase in occurrence space and adsorption capacity is less. In this case, the Langmuir equation was not suitable for the expression of adsorption capacity of columnar samples.

In the low-pressure stage, the adsorption capacity of powdered coal samples is higher than that of columnar coal samples. The isotherm adsorption curves of 60−80 and 200 mesh coal samples from CZ are basically coincidental. However, the adsorption capacity of 200 mesh coal samples from WY and YJL is higher than that of 60−80 mesh coal samples. These observations showed that the adsorption capacity of coal increased with the decrease in particle size, which was related to the connectivity of pores and fissures in the coal. When the coal sample was crushed, the SSA and the effective storage space of gas increased. For columnar samples, the path and time of gas migration to the micropore surface were longer, so the adsorption capacity was relatively smaller.

According to the Langmuir equation, the isothermal adsorption data of each coal sample was fitted. Consequently, the adsorption constants a, b, and correlation coefficient (R^2) were obtained. The results are shown in Table 3.

In Table 3, a is the Langmuir volume, which represents the maximum adsorption volume of the coal sample in the dry state. b is the adsorption constant, which is the reciprocal of

Table 3. Fitting Results of Isothermal Adsorption Constants[a]

sample number	sample size	a ($cm^3 \cdot g^{-1}$)	b (MPa^{-1})	R^2
CZ-200	200 mesh	43.1071	1.0686	0.9892
CZ-60	60−80 mesh	44.6449	1.1292	0.9927
CZ-C	columnar	50.7840	9.0967	0.9990
WY-200	200 mesh	50.7870	3.0702	0.9743
WY-60	60−80 mesh	40.7916	2.6598	0.9848
WY-C	columnar	42.2262	4.6748	0.9719
YJL-200	200 mesh	63.8162	7.8625	0.9927
YJL-60	60−80 mesh	41.6039	6.1419	0.9830
YJL-C	columnar	32.5195	5.5979	0.8040

[a]Note: a, the Langmuir volume ($cm^3 \cdot g^{-1}$); b, the reciprocal of Langmuir pressure (MPa^{-1}).

https://doi.org/10.1021/acsomega.1c02442
ACS Omega 2021, 6, 19115−19126

Table 4. Adsorption Capacity and Pore Characteristics of Coal Samples[a]

sample number	HP-CH_4GA ($cm^3 \cdot g^{-1}$)	V_{CO2}	S_{CO2}	V_{Ar1}	S_{Ar1}	V_{Ar2}	S_{Ar2}	V_{CO2+Ar}	S_{CO2+Ar}
CZ	44.6449	0.0890	304.99	0.0008	0.33	0.0008	0.036	0.091	305.35
WY	40.7916	0.0560	178.71	0.0009	0.26	0.0015	0.061	0.058	179.03
YJL	41.6039	0.0620	208.91	0.0210	17.30	0.0075	0.35	0.091	226.55

[a]Note: V_{CO2}, V_{Ar1}, V_{Ar2}, and V_{CO2+Ar} are the cumulative PV values of 0.3−1.5, 1.5−30, 30−230, and 0.3−230 nm, respectively ($cm^3 \cdot g^{-1}$). S_{CO2}, S_{Ar1}, S_{Ar2}, S_{CO2+Ar} are the cumulative SSA values of 0.3−1.5, 1.5−30, 30−230, and 0.3−230 nm, respectively ($m^2 \cdot g^{-1}$).

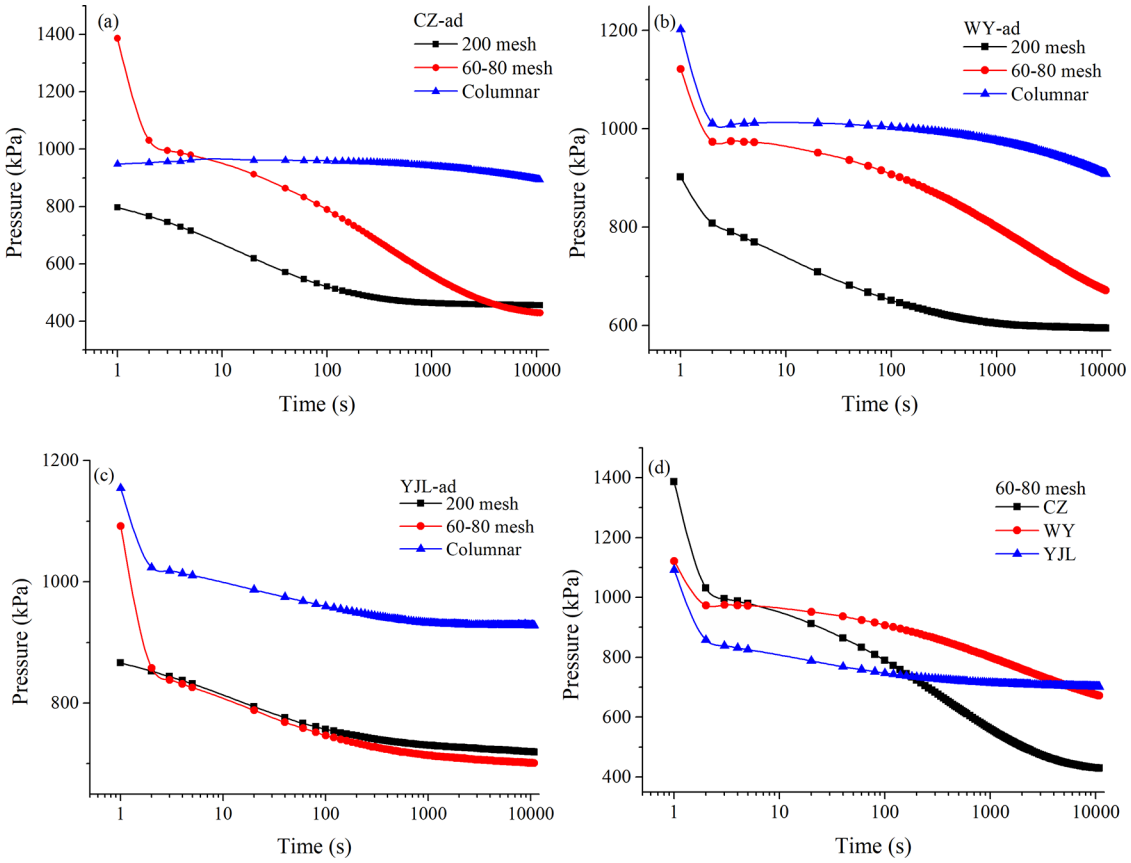

Figure 4. Pressure change curves versus time. (a) Three kinds of coal samples from CZ. (b) Three kinds of coal samples from WY. (c) Three kinds of coal samples from YJL. (d) 60−80 mesh coal samples from CZ, WY, and YJL.

the Langmuir pressure. The maximum adsorption capacities (i.e., *a*) of 60−80 mesh coal samples from CZ, WY, and YJL are 44.6449, 40.7916, and 41.6039 $cm^3 \cdot g^{-1}$, respectively. Accordingly, the adsorption constants (i.e., *b*) are 1.1292, 2.6598, and 6.1419 MPa^{-1}, respectively. This indicated that the metamorphic degree had a major impact on the distribution characteristics and connectivity of the pores in the coal. Under metamorphism, new pores will appear in the coal. At the same time, under the action of pressure for a long time, the pores and fissures in the coal had been deformed, which eventually affected the adsorption capacity of the coal. The maximum adsorption capacity of 200 and 60−80 mesh coal samples from CZ is basically close, while the maximum adsorption capacity of 200 mesh coal samples from WY and YJL is higher than that of 60−80 mesh coal samples. These results indicated that the effective migration path and adsorption space of nanopores in the coal increased with the decrease in coal particle size. The adsorption capacity was related to the type and development scale of nanopores, especially micropores.[17]

3.2.2. Influence of Development Characteristics of Nanopores on Adsorption Capacity. The development scale, morphology, and distribution characteristics of nanopores in the coal will affect the behavior and scale of gas adsorption and migration. To explore the intrinsic relationship between nanopores and gas adsorption and migration, LP-CA and LP-AA experiments were performed on 60−80 mesh coal samples. The pore structure of these coal samples is analyzed using the models in Table 1. Related studies found that the BJH model was underestimated in the analysis of nanopores with a pore size of less than 10 nm.[3] According to the common pitfalls and limitations of the analysis models, the pore information of 0.3−1.5 nm was analyzed by LP-CA with the NLDFT model. The pore information of 1.5−30 and 30−230 nm was obtained by LP-AA combined with the QSDFT and BJH model, respectively. The analysis results are shown in Table 4.

In Table 4, the cumulative PV values of CZ, WY, and YJL coal samples at 0.3−230 nm are 0.091, 0.058, and 0.091 $cm^3 \cdot g^{-1}$, respectively, and the corresponding cumulative SSA values of pores are 305.35, 179.03, and 226.55 $m^2 \cdot g^{-1}$, respectively. There was a positive correlation between the cumulative SSA of pores and the adsorption capacity of coal samples. In

https://doi.org/10.1021/acsomega.1c02442
ACS Omega 2021, 6, 19115−19126

Table 5. Calculation Results of Coal Sample Adsorption Parameters[a]

sample number	V_a ($cm^3 \cdot g^{-1}$)	V_a/P_a ($cm^3 \cdot g^{-1} \cdot MPa^{-1}$)	5 s (%)	10 min (%)	40 min (%)	180 min (%)
CZ-200	13.96	33.03	45.16	96.23	98.05	98.76
CZ-60	13.90	31.01	7.23	68.98	88.85	98.53
CZ-Z	4.69	5.99		0.04	11.87	32.33
WY-200	12.29	19.15	53.22	94.40	97.59	98.63
WY-60	10.38	16.33	7.20	47.43	68.84	90.17
WY-Z	7.41	9.46		10.39	22.86	44.69
YJL-200	6.88	9.70	49.51	89.94	93.20	95.87
YJL-60	6.09	8.72	42.41	91.24	96.15	99.14
YJL-Z	7.22	7.73	33.50	99.16	104.95	106.17

[a]Note: V_a, adsorption capacity; P_a, adsorption pressure; V_a/P_a, the adsorption capacity under unit pressure.

particular, the contribution of the total SSA of 0.3−1.5 nm micropores was more significant. The development characteristics of micropores in the coal were verified to play a key role in the gas adsorption capacity, which was consistent with the previous research results.[34]

3.2.3. Influence of Pore Connectivity on Gas Migration. The speed and scale of gas adsorption and migration were not only related to the development scale of nanopores but also related to the connectivity of nanopores, including the nanopores inside and between nanopores and adjacent fissures. To explore the influence of pore connectivity on gas migration, the powdered and columnar coal samples were chosen for isothermal adsorption experiments. The two kinds of coal samples were the sampled same layers. The development scale of nanopores in these samples was similar, while the connectivity was obviously different. The curves of pressure versus time for each coal sample are drawn according to the original data recorded in the equilibrium process when the target pressure is 1 MPa in the isothermal adsorption experiment. Details are shown in Figure 4.

From Figure 4, the curves of pressure versus time of different coal samples have both similarities and differences. In the same place, the shape of pressure curves of powdered coal samples is obviously different from that of columnar coal samples. The shape of powdered coal samples with different particle sizes is similar, but the degree of pressure reduction is similar (Figure 4c) or obvious (Figure 4a,b). When high-pressure methane was filled into the sample cylinder, the pressure reached the maximum rapidly and then decreased gradually with the extension of adsorption time. In addition, the decrease amplitude was obvious in the initial stage. In this process, the gas first entered the large connected fissures and then the micro-fissures and nanopores in turn, resulting in a significant decrease in the recorded gas pressure. The gas migration speed and scale were relatively large (Figure 4d). When the particle size of coal samples increased, the pressure reduction range and speed were relatively slow, indicating that the gas passed through the connected fissures, micro-fissures, and nanopores to reach the adsorption site on the surface of nanopores. Therefore, the migration path of gas increased and the time to reach adsorption equilibrium was prolonged (Figure 4a−c). The pressure curves of 60−80 mesh coal samples in different places had significant differences in shape, reduction amplitude, and speed (Figure 4d), suggesting that the pore development characteristics were different as well.

To quantitatively describe the scale of gas migration, the instantaneous adsorption capacity at different times and the absolute adsorption capacity at adsorption equilibrium of each coal sample were calculated by using the above calculation method.[32] To indicate the effect of pressure propagation on adsorption migration, the absolute adsorption capacity at equilibrium was divided by the equilibrium pressure to obtain the adsorption capacity per unit pressure (V_a/P_a). The calculation results are shown in Table 5.

In Table 5, as the particle size of coal samples from the same sampling position decreases, the adsorption capacity and V_a/P_a exhibit an overall increasing trend. This showed that the gas in the coal samples with a large particle size overcame greater resistance to pass the adsorption position in the micropores through the micro-fissures and nanopores. The proportion of gas adsorption at different times showed that the adsorption capacity of all coal samples increased gradually with the increase in adsorption time until it was close to the equilibrium adsorption capacity. To quantitatively describe the speed of gas migration, the adsorption efficiency was defined as instantaneous adsorption capacity divided by equilibrium adsorption capacity, expressed as a percentage.

When the adsorption time is 5 s, CZ and WY columnar coal samples do not have effective adsorption while the adsorption efficiency of YJL columnar coal sample reaches 33.50%. When the adsorption time is 10 min, the adsorption efficiency of all coal samples increases and the adsorption efficiency of powdered coal samples is higher than that of columnar coal samples. The rate and scale of gas adsorption and migration decreased with the increase in coal particle size.

It was worth noting that the adsorption efficiency of 200 mesh coal samples from YJL is lower than those of 200 mesh coal samples from CZ and WY. In addition, when the adsorption times are 40 and 180 min, the adsorption efficiency of the YJL columnar coal sample is more than 100%. This was due to the good development and connectivity of micro-fissures and nanopores in the YJL coal samples. In the initial stage, the gas entered the fissures and micro-fissures rapidly and the pressure decreased obviously. When the adsorption time is 10 min, the adsorption efficiency reaches 90%. As more and more gases entered the micropores, the gas concentration in the micropores was higher than the equilibrium concentration, thus resulting in supersaturated adsorption. The concentration inside and outside the micropores tended to be the same over the adsorption time and finally reached the equilibrium state. The speed and scale of gas migration were not only related to the connectivity of pores and fissures but also related to the deformation degree.

3.3. Analysis of Deformation Characteristics of the Nanopore Structure. By weighing the coal samples before and after adsorption−desorption, the weight is more than the original coal samples. At the same time, the serious swell deformation of columnar coal samples made them difficult to

https://doi.org/10.1021/acsomega.1c02442
ACS Omega 2021, 6, 19115−19126

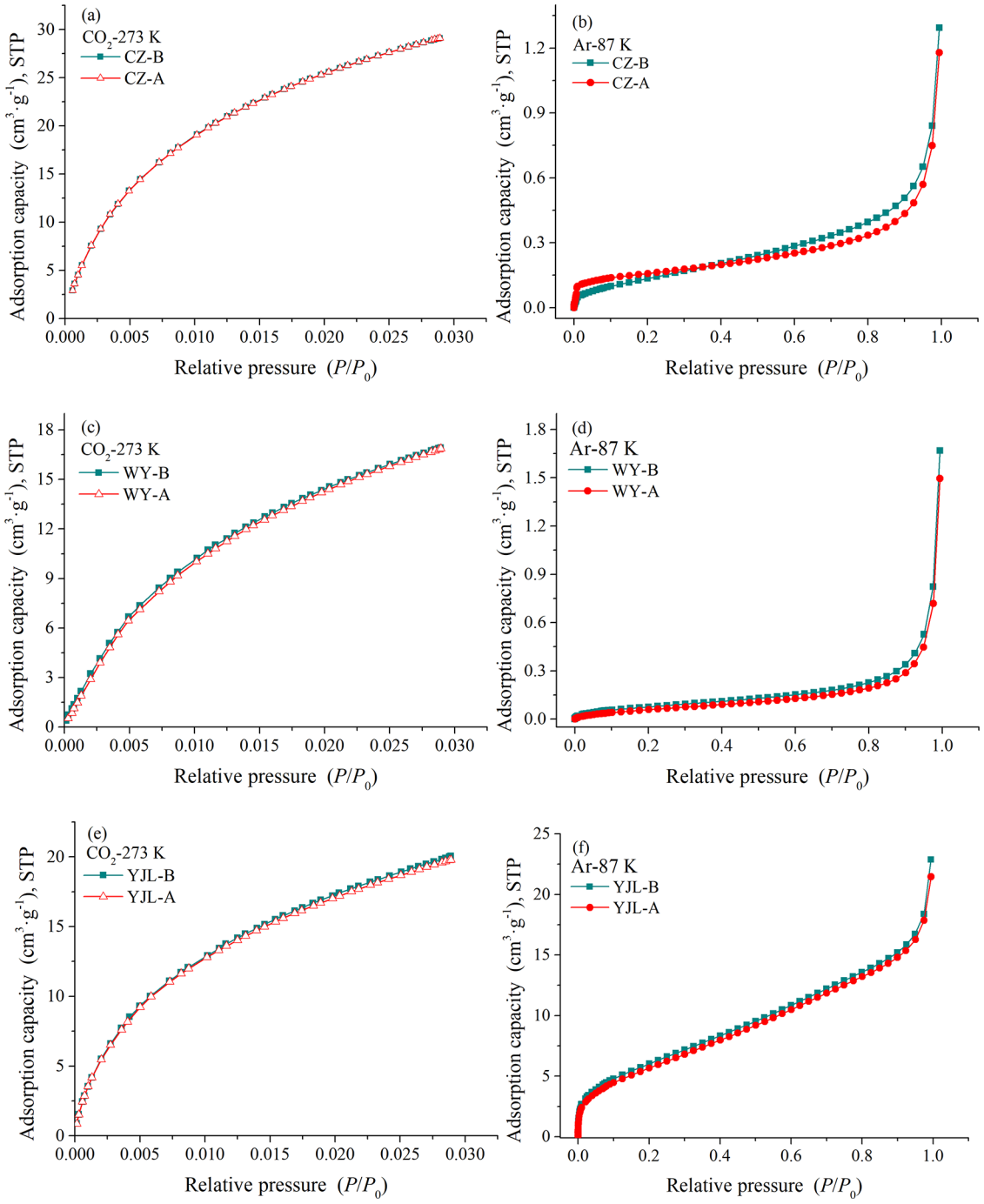

Figure 5. Low-pressure adsorption curves. (a, c, e) Adsorption curves of LP-CA. (b, d, f) Adsorption curves of LP-AA.

remove. These results indicated that some of the gas remained in the coal after gas desorption. Previous research found that the coal matrix will swell or shrink after gas adsorption−desorption, and the pore structure and distribution characteristics of coal will change.[36] In this part, the pore structure of low-pressure gas adsorption was tested. Meanwhile, the deformation characteristics of different types of nanopores were analyzed.

3.3.1. Analysis of the Difference of Low-Pressure Adsorption Curves. The pore structure of three kinds of coal samples (60−80 mesh) before and after adsorption−desorption was determined by LP-CA and LP-AA methods. Then, the low-pressure adsorption curves are obtained, as shown in Figure 5.

From Figure 5, CZ-B, WY-B, and YJL-B represent the coal samples before adsorption; CZ-A, WY-A, and YJL-A represent the coal samples after adsorption−desorption. The LP-CA adsorption curves of coal samples after adsorption−desorption basically coincide with those of coal samples before adsorption (Figure 5a) or slightly decrease (Figure 5c,e). The shape of the LP-AA adsorption curves basically remains unchanged, while the maximum adsorption value of Ar reduces slightly (Figure 5b,d,f). These indicated that the pore structure and distribution characteristics of coal samples had changed after adsorption−desorption. The significant differences in the

https://doi.org/10.1021/acsomega.1c02442
ACS Omega 2021, 6, 19115−19126

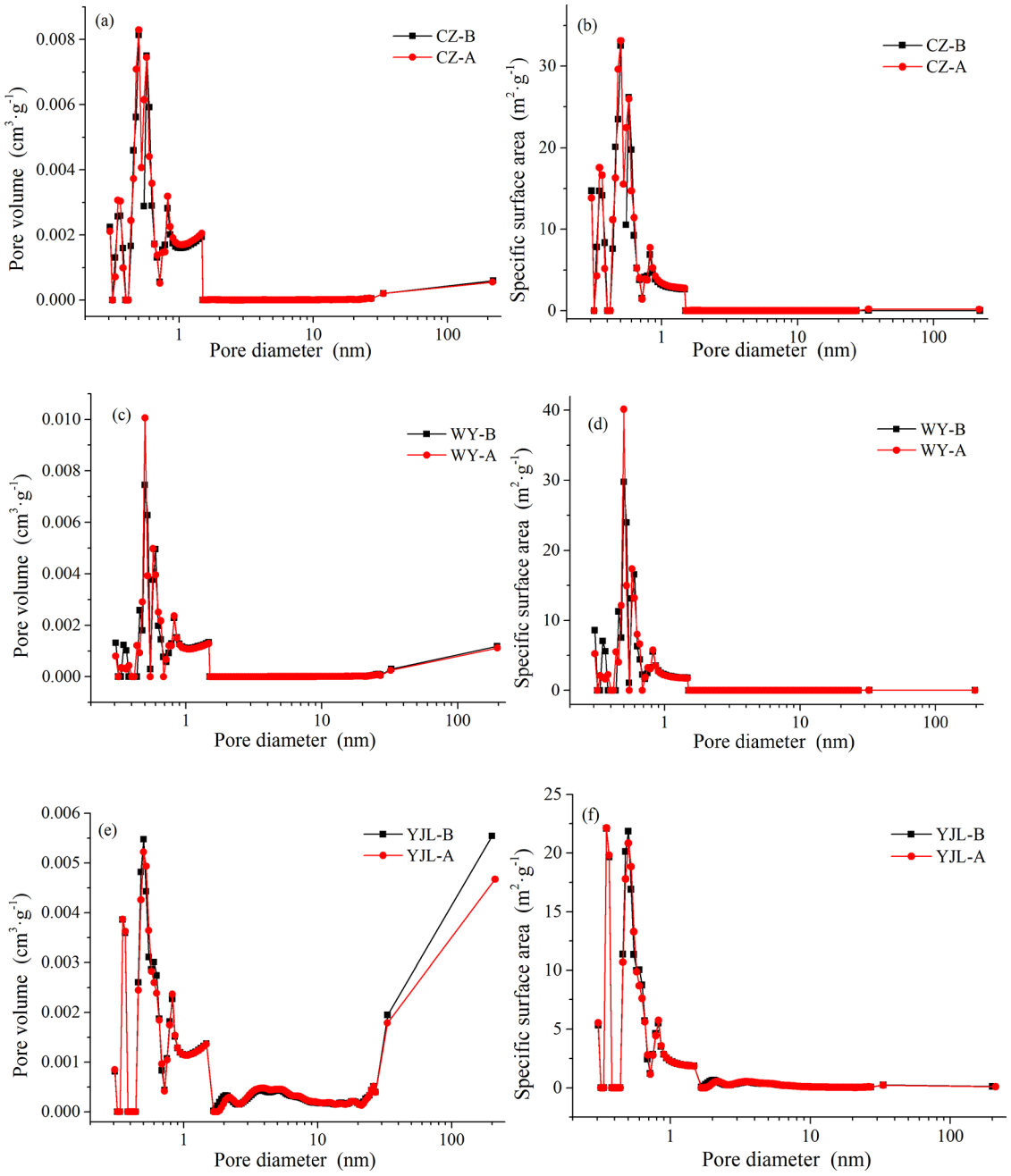

Figure 6. Distribution curves of PV and SSA. (a, c, e) PV curves of coal samples from CZ, WY, and YJL, respectively. (b, d, f) SSA curves of coal samples from CZ, WY, and YJL, respectively.

shape of LP-AA adsorption curves between coal samples indicated that the development scale and distribution of nanopores were also markedly different.

3.3.2. Analysis of Changes in the Nanopore Structure. To analyze the change characteristics of the nanopore structure in the coal samples after adsorption−desorption, the PV and SSA curves between 0.3 and 230 nm were obtained by using the analysis model mentioned earlier in this paper, as shown in Figure 6.

From Figure 6, the distribution curve shape of PV and SSA for all the coal samples after adsorption−desorption is basically consistent and the pore concentration section remains unchanged. The distribution curves of PV and SSA of coal samples in different places are obviously different, which is the fundamental reason for the different migration scale and speed of gas adsorption. The PV and SSA of coal samples with the same pore size had many forms, such as almost unchanged, increased, or decreased, which was due to the swell or shrinkage deformation of the coal matrix and the collaborative or partial deformation of nanopores.

The contribution of different types of pores to the total PV and SSA was different. The micropores of CZ and WY coal samples contribute the most to the total PV and SSA. By comparison, the micropores, mesopores, and macropores of YJL coal samples contribute to the total PV and the total SSA mainly comes from micropores and mesopores. The accumulative PV and SSA of different types of nanopores are shown in Figure 7.

From Figure 7, the cumulative deformation of the nanopore structure in the coal is anisotropic. The total PV of CZ coal

https://doi.org/10.1021/acsomega.1c02442
ACS Omega 2021, 6, 19115−19126

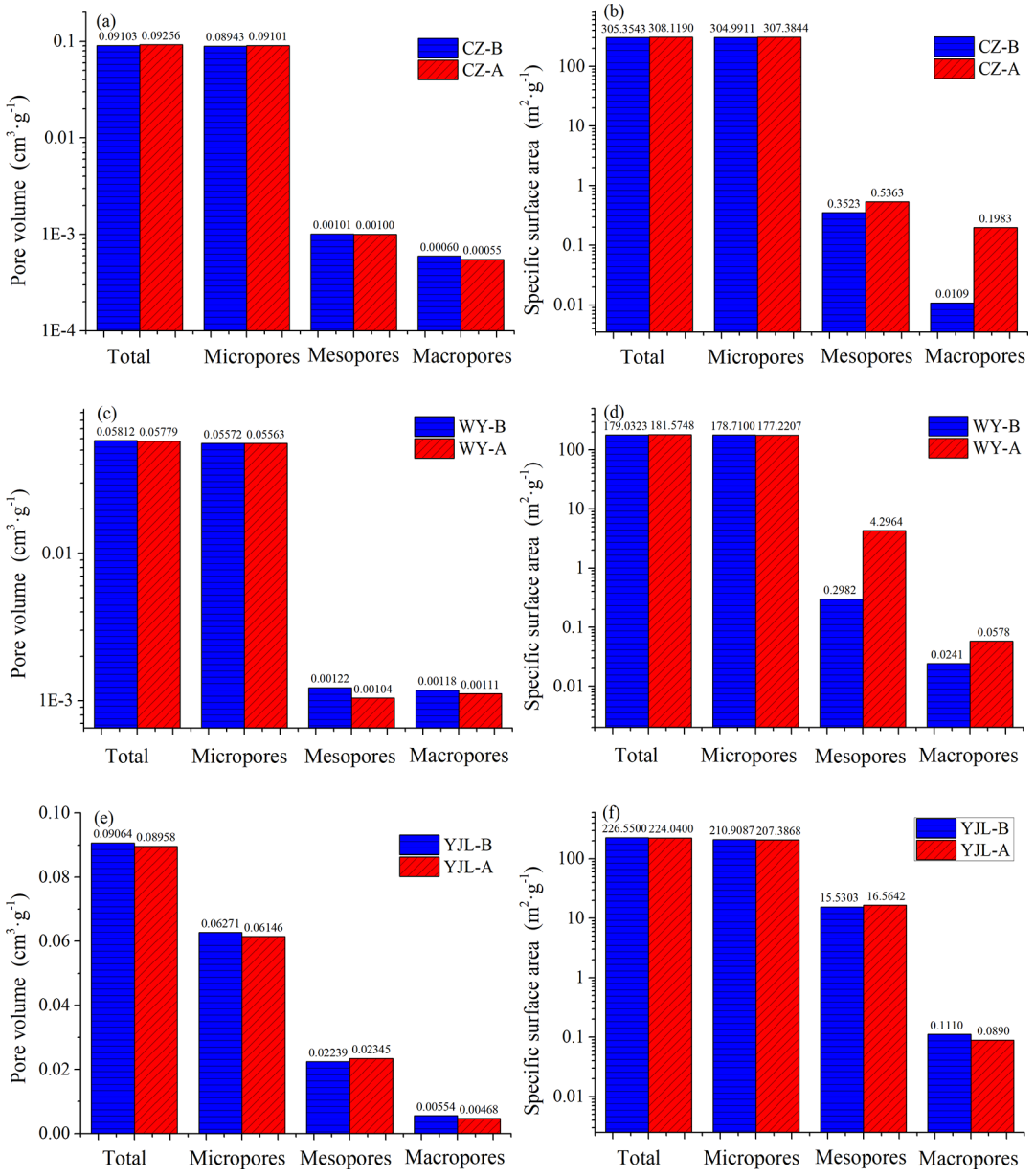

Figure 7. PV and SSA of nanopores at different types. (a, c, e) Cumulative PV of coal samples from CZ, WY, and YJL, respectively. (b, d, f) Cumulative SSA of coal samples from CZ, WY, and YJL, respectively.

samples increases from 0.09103 to 0.09256 $cm^3 \cdot g^{-1}$, which is caused by the increase in the PV of micropores by 0.001582 $cm^3 \cdot g^{-1}$. On the contrary, the PV values of mesopores and macropores decrease by 0.00001 and 0.00005 $cm^3 \cdot g^{-1}$, respectively (Figure 7a). The total SSA of pores increases from 305.3543 to 308.1190 $m^2 \cdot g^{-1}$, and the SSA values of micropores, mesopores, and macropores increase by 2.3933, 0.1839, and 0.1875 $m^2 \cdot g^{-1}$, respectively (Figure 7b).

The total PV of WY coal samples decreases from 0.05812 to 0.05779 $cm^3 \cdot g^{-1}$. The PV values of micropores, mesopores, and macropores decrease by 0.00008, 0.00018, and 0.00006 $cm^3 \cdot g^{-1}$, respectively (Figure 7c). The total SSA of pores increases from 179.0323 to 181.5748 $m^2 \cdot g^{-1}$. The SSA values of mesopores and macropores increase by 3.9982 and 0.0336 $m^2 \cdot g^{-1}$, respectively, while the SSA of micropores decreases by 1.4893 $m^2 \cdot g^{-1}$ (Figure 7d).

The total PV of YJL coal samples decreases from 0.09064 to 0.08958 $cm^3 \cdot g^{-1}$. The PV values of micropores and macropores decrease by 0.00125 and 0.00087 $cm^3 \cdot g^{-1}$, respectively. Instead, the PV of mesopores increases by 0.00105 $cm^3 \cdot g^{-1}$ (Figure 7e). The total SSA of pores decreases from 226.55 to 224.04 $m^2 \cdot g^{-1}$. The SSA values of micropores and macropores decrease by 3.5219 and 0.0220 $m^2 \cdot g^{-1}$, respectively, while that of mesopores increases by 1.0339 $m^2 \cdot g^{-1}$ (Figure 7f).

After adsorption−desorption, the nanopore structure in the coal swelled or shrunk, and the PSD changed as well. In the three coal samples, the PV of macropores decreased, while the SSA of mesopores increased (Figure 7). Relevant researchers also found that the coal had non-uniform expansion deformation after methane adsorption through CT and SEM experiments on coal samples.[26]

3.3.3. Deformation Mechanism of the Pore Structure and Its Significance to CBM Development. The coal matrix will swell or shrink after gas adsorption−desorption, which belongs to the residual deformation caused by the "lag effect". These two kinds of deformation will change the distribution

https://doi.org/10.1021/acsomega.1c02442
ACS Omega 2021, 6, 19115−19126

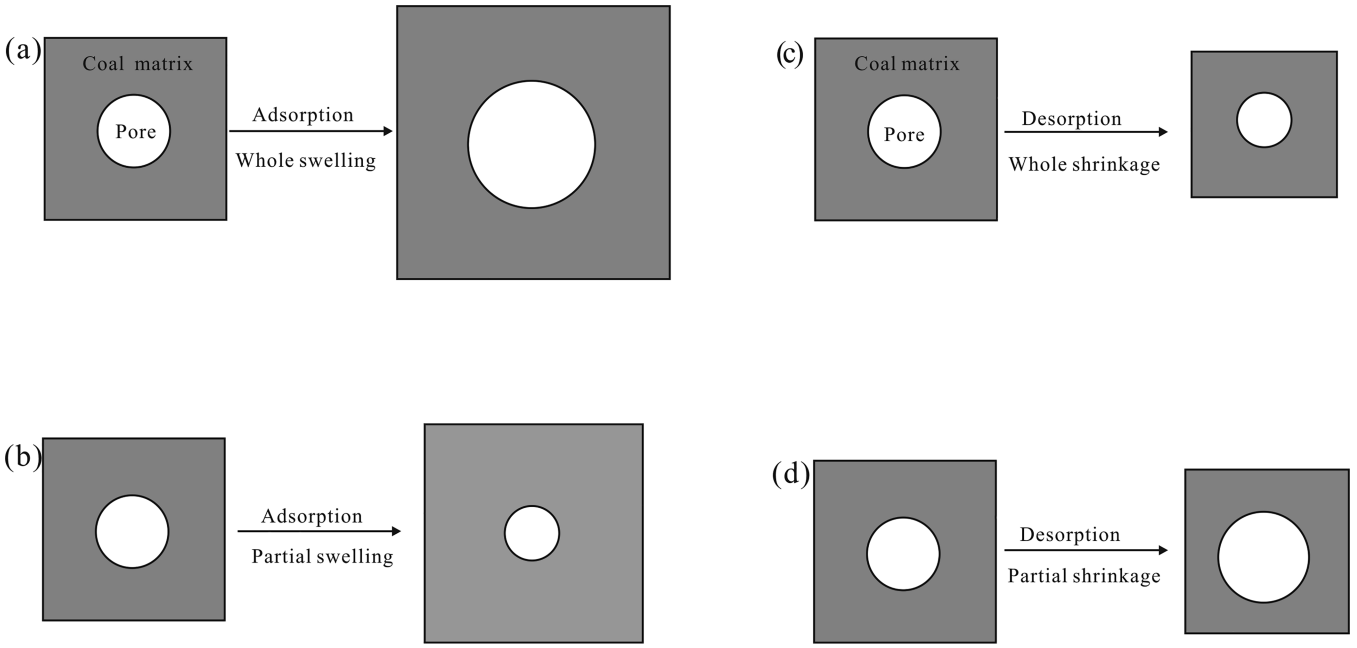

Figure 8. (a–d) Pore structure deformation mechanism.

characteristics of nanopores, micro-fissures, and fissures nearby. There are two types of deformation mechanisms: the whole collaborative deformation and partial deformation. The pore structure deformation mechanisms are shown in Figure 8.

From Figure 8, one of the deformation mechanisms is the whole collaborative deformation: after the coal matrix adsorption gas, the pores and the matrix swell and deform together. Therefore, the pore becomes larger (Figure 8a). Similarly, after the coal matrix desorption gas, the coal matrix and pores will shrink and deform as a whole and thus the pore becomes smaller (Figure 8c). In Figure 6e,f, the volume and surface area of some pores decrease, which is consistent with this deformation mechanism.

The other is the partial deformation: the coal matrix swells after adsorption, some of the matrix around the pores swells more obviously, and the pore becomes smaller (Figure 8b). Similarly, after the coal matrix desorption gas, the partial shrinkage deformation of the coal matrix around other pores is remarkable, and the pore will become larger (Figure 8d). In Figure 6c,d, the volume and surface area of some pores present a tendency of increasing, which is consistent with this deformation mechanism.

Therefore, in the process of CBM desorption and migration, pores and fissures may be deformed, especially affecting the initial gas migration speed and scale, thus affecting the recovery of CBM. In the in situ state, most of the CBM was adsorbed on the surface of micropores in the coal. The pressure of free gas inside and outside the nanopores was in a dynamic equilibrium state, and the gas concentration inside and outside the nanopores was equal. When the dynamic equilibrium of pressure or concentration was broken, the gas on the micropore surface will be desorbed and diffused and then migrated to the connected nanopores.

The desorption and migration of gas will change the size and structure of nanopores, thus affecting change in the form and scale of gas migration in pores. This will further influence the gas migration scale and gas production potential in micro-fissures.[37] The well development and connectivity of nanopores are beneficial to the storage and migration of CBM (such as YJL coal samples). In the process of gas production, the effective stress of the coal reservoir decreases with time. The fissures will have a double deformation mechanism of opening or closing after force action and gas desorption, and the gas seepage capacity will change. Therefore, to improve the yield rate of CBM, more attention should be paid to the deformation control on the structure of nanopores and fissures, fine fracturing, and drainage control from the nanoscale during CBM development.

4. CONCLUSIONS

To investigate the influence of the nanopore structure on the occurrence and migration of CBM, proximate analysis, vitrinite reflectance, and HP-CH_4GA, LP-CA, and LP-AA tests were performed with evaluating adsorption and nanopore characteristics of the coal with different particle sizes from three places. The change characteristics of nanopores of coal samples before and after high-pressure adsorption were compared and analyzed. The main conclusions were as follows.

The results of high-pressure gas adsorption showed that the adsorption data of powdered and columnar coal samples in a low-pressure stage (<8 MPa) were highly fitted with the Langmuir equation, and the adsorption capacity of powdered coal samples was higher than that of columnar coal samples. When the gas pressure was higher than 8 MPa, some adsorption data deviated from the original fitting curve, which was more obvious in columnar coal samples. Generally, the maximum adsorption capacity of the powdered coal sample was higher than that of columnar coal samples.

The LP-CA and LP-AA test results showed that the cumulative PV values of CZ, WY, and YJL coal samples at 0.3–230 nm were 0.091, 0.058, and 0.091 $cm^3 \cdot g^{-1}$, respectively. In addition, the corresponding cumulative SSA values of pores were 305.35, 179.03, and 226.55 $m^2 \cdot g^{-1}$, respectively. There was a positive correlation between the cumulative SSA of pores and the adsorption capacity of coal samples.

https://doi.org/10.1021/acsomega.1c02442
ACS Omega 2021, 6, 19115–19126

The curves of pressure versus time showed that the pressure decreased obviously in the initial stage. When the particle size of coal samples increased, the pressure reduction range and speed were relatively slow, which indicated that the rate and scale of gas adsorption and migration decreased.

The results of the pore structure test showed that the adsorption curves of LP-CA remained basically unchanged or decreased slightly. In contrast, the shape of LA-AA adsorption curves remained unchanged, but the maximum adsorption value of Ar decreased.

After adsorption−desorption, the nanopore structure in the coal swelled or shrunk, and the PSD also changed. The cumulative deformation of the nanopore structure was anisotropic. There were two types of deformation: the whole collaborative deformation and partial deformation. Both gas adsorption and desorption could result in the shrinkage or swell deformation of nanopores and fissures, thus affecting the production of CBM.

AUTHOR INFORMATION

Corresponding Author

Xiaofeng Ji − *School of Energy and Materials Engineering, Taiyuan University of Science and Technology, Taiyuan 030024, P. R. China; Institute of Resource and Environment, Henan Polytechnic University, Jiaozuo 454000, P. R. China;* orcid.org/0000-0002-4609-6744; Email: xiaofengji@tyust.edu.cn

Authors

Dangyu Song − *Institute of Resource and Environment, Henan Polytechnic University, Jiaozuo 454000, P. R. China;* orcid.org/0000-0001-5906-0161

Wenfang Shi − *School of Materials Science and Engineering, Taiyuan University of Science and Technology, Taiyuan 030024, P. R. China*

Yanfei Li − *Shanxi Province Mineral Resources Investigation and Monitoring Center, Taiyuan 030024, P. R. China*

Complete contact information is available at: https://pubs.acs.org/10.1021/acsomega.1c02442

Notes

The authors declare no competing financial interest.

ACKNOWLEDGMENTS

This work was supported by the Applied Basic Research Plan of Shanxi Province (No. 201901D211294), Universities Science and Technology Innovation Project in Shanxi Province (No. 2019L0641 and 2020L0365), Ph.D. Research Launch Fund of Taiyuan University of Science and Technology (No. 20192073), Reward Fund for Excellent Doctors Working in Shanxi Province (No. 20192074), and College Students Innovation and Entrepreneurship Training Program of Taiyuan University of Science and Technology (No. XJ2020178). We would like to express our appreciation to the other members of the laboratory for the help provided in experiments and language editing.

REFERENCES

(1) Cai, Y.; Liu, D.; Pan, Z.; Yao, Y.; Li, J.; Qiu, Y. Pore structure and its impact on CH_4 adsorption capacity and flow capability of bituminous and subbituminous coals from Northeast China. *Fuel* **2013**, *103*, 258−268.

(2) Ho, C. K.; Webb, S. W. *Gas Transport in Porous Media*; Springer: Netherlands, 2006; pp. 1−2.

(3) Thommes, M.; Kaneko, K.; Neimark, A. V.; Olivier, J. P.; Rodriguez-Reinoso, F.; Rouquerol, J.; Sing, K. S. W. Physisorption of gases, with special reference to the evaluation of surface area and pore size distribution (IUPAC Technical Report). *Pure Appl. Chem.* **2015**, *87*, 1051−1069.

(4) Li, X.; Fu, X.; Liu, A.; An, H.; Wang, G.; Yang, X.; Wang, L.; Wang, H. Methane adsorption characteristics and adsorbed gas content of low-rank coal in china. *Energy Fuels* **2016**, *30*, 3840−3848.

(5) Song, D.; Ji, X.; Li, Y.; Zhao, H.; Song, B.; He, K. Heterogeneous development of micropores in medium-high rank coal and its relationship with adsorption capacity. *Int. J. Coal Geol.* **2020**, *226*, 103497.

(6) Jiang, J.; Yang, W.; Cheng, Y.; Zhao, K.; Zheng, S. Pore structure characterization of coal particles via MIP, N_2 and CO_2 adsorption: Effect of coalification on nanopores evolution. *Powder Technol.* **2019**, *354*, 136−148.

(7) Zhao, J.; Qin, Y.; Shen, J.; Zhou, B.; Li, G.; Li, G. Effects of pore structures of different maceral compositions on methane adsorption and diffusion in anthracite. *Appl. Sci.* **2019**, *9*, 5130.

(8) Kwiecińska, B.; Pusz, S.; Valentine, B. J. Application of electron microscopy TEM and SEM for analysis of coals, organic-rich shales and carbonaceous matter. *Int. J. Coal Geol.* **2019**, *211*, 103203.

(9) Song, S. B.; Liu, J. F.; Yang, D. S.; Ni, H. Y.; Huang, B. X.; Zhang, K.; Mao, X. B. Pore structure characterization and permeability prediction of coal samples based on SEM images. *J. Nat. Gas Sci. Eng.* **2019**, *67*, 160−171.

(10) Yao, Y.; Liu, D. Comparison of low-field NMR and mercury intrusion porosimetry in characterizing pore size distributions of coals. *Fuel* **2012**, *95*, 152−158.

(11) Fan, N.; Wang, J.; Deng, C.; Fan, Y.; Wang, T.; Guo, X. Quantitative characterization of coal microstructure and visualization seepage of macropores using CT-based 3D reconstruction. *J. Nat. Gas Sci. Eng.* **2020**, *81*, 103384.

(12) Radlinski, A. P.; Mastalerz, M.; Hinde, A. L.; Hainbuchner, M.; Rauch, H.; Baron, M.; Lin, J. S.; Fan, L.; Thiyagarajanf, P. Application of SAXS and SANS in evaluation of porosity, pore size distribution and surface area of coal. *Int. J. Coal Geol.* **2004**, *59*, 245−271.

(13) Okolo, G. N.; Everson, R. C.; Neomagus, H. W. J. P.; Roberts, M. J.; Sakurovs, R. Comparing the porosity and surface areas of coal as measured by gas adsorption, mercury intrusion and SAXS techniques. *Fuel* **2015**, *141*, 293−304.

(14) Li, Y. H.; Lu, G. Q.; Rudolph, V. Compressibility and fractal dimension of fine coal particles in relation to pore structure characterisation using mercury porosimetry. *Part. Part. Syst. Charact.* **1999**, *16*, 25−31.

(15) Kuila, U.; Prasad, M. Specific surface area and pore-size distribution in clays and shales. *Geophys. Prospect.* **2013**, *61*, 341−362.

(16) Zhao, Y.; Sun, Y.; Liu, S.; Chen, Z.; Yuan, L. Pore structure characterization of coal by synchrotron radiation nano-CT. *Fuel* **2018**, *215*, 102−110.

(17) Crosdale, P. J.; Beamish, B. B.; Valix, M. Coalbed methane sorption related to coal composition. *Int. J. Coal Geol.* **1998**, *35*, 147−158.

(18) Krooss, B. M.; Van Bergen, F.; Gensterblum, Y.; Siemons, N.; Pagnier, H. J. M.; David, P. High-pressure methane and carbon dioxide adsorption on dry and moisture-equilibrated Pennsylvanian coals. *Int. J. Coal Geol.* **2002**, *51*, 69−92.

(19) Cai, T.; Feng, Z.; Jiang, Y.; Zhao, D. Thermodynamic characteristics of methane adsorption of coal with different initial gas pressures at different temperatures. *Adv. Mater. Sci. Eng.* **2019**, 1−9.

(20) Jia, T.; Liu, C.; Wei, G.; Yan, J.; Zhang, Q.; Niu, L.; Liu, X.; Zhang, M.; Ju, Y.; Zhang, Y. Micro-nanostructure of coal and adsorption-diffusion characteristics of methane. *J. Nanosci. Nanotechnol.* **2021**, *21*, 422−430.

(21) Pan, J.; Zhao, Y.; Hou, Q.; Jin, Y. Nanoscale pores in coal related to coal rank and deformation structures. *Transp. Porous Med.* **2015**, *107*, 543−554.
(22) Liu, X.; He, X. Effect of pore characteristics on coalbed methane adsorption in middle-high rank coals. *Adsorption* **2017**, *23*, 3−12.
(23) Yi, M.; Cheng, Y.; Wang, Z.; Wang, C.; Hu, B.; He, X. Effect of particle size and adsorption equilibrium time on pore structure characterization in low pressure N_2 adsorption of coal: an experimental study. *Adv. Powder Technol.* **2020**, *31*, 4275−4281.
(24) Zhang, H.; Diao, R.; Chan, H. H.; Mostofi, M.; Evans, B. Molecular simulation of the adsorption-induced deformation during CO_2 sequestration in shale and coal carbon slit pores. *Fuel* **2020**, *272*, 117693.
(25) Zhu, W. C.; Wei, C. H.; Liu, J.; Xu, T.; Elsworth, D. Impact of gas adsorption induced coal matrix damage on the evolution of coal permeability. *Rock Mech. Rock Eng.* **2013**, *46*, 1353−1366.
(26) Feng, Z.; Zhou, D.; Zhao, Y.; Cai, T. Study on microstructural changes of coal after methane adsorption. *J. Nat. Gas Sci. Eng.* **2016**, *30*, 28−37.
(27) Feng, Y. Y.; Yang, W.; Chu, W. Coalbed methane adsorption and desorption characteristics related to coal particle size. *Chin. Phys. B* **2016**, *25*, No. 068102.
(28) Zhang, L.; Aziz, N.; Ren, T.; Nemcik, J.; Tu, S. Influence of coal particle size on coal adsorption and desorption characteristics. *Arch. Min. Sci.* **2014**, *59*, 807−820.
(29) Standardization Administration of China *Proximate Analysis of Coal-Instrumental method*; GB/T 30732−2014; China National Standards: Beijing, China, 2014.
(30) Standardization Administration of China *Method of Determining Microscopically the Reflectance of Vitrinite in Coal*; GB/T 6948−2008; China National Standards: Beijing, China, 2008.
(31) Standardization Administration of China *Experimental Method of High-Pressure Isothermal Adsorption to Coal*; GB/T 19560−2008; China National Standards: Beijing, China, 2008.
(32) Mavor, M. J.; Owen, L. B.; Pratt, T. J. Measurement and Evaluation of Coal Sorption Isotherm Data. *SPE Annual Technical Conference and Exhibition*; OnePetro: New Orleans, Louisiana, September 1990.
(33) Standardization Administration of China *Pore Size Distribution and Porosity of Solid Materials by Mercury Porosimetry and Gas Adsorption-Part 2: Analysis of Mesopores and Macropores by Gas Adsorption*; GB/T 21650.2−2008; China National Standards: Beijing, China, 2008.
(34) Standardization Administration of China *Pore Size Distribution and Porosity of Solid Materials by Mercury Porosimetry and Gas Adsorption-Part 3: Analysis of Micropores by Gas Adsorption*; GB/T 21650.3−2011; China National Standards: Beijing, China, 2011.
(35) Langmuir, I. The constitution and fundamental properties of solids and liquids. Part I. solids. *J. Am. Chem. Soc.* **1916**, *38*, 102−105.
(36) Ji, X.; Song, D.; Ni, X.; Li, Y.; Zhao, H. Coal matrix deformation and pore structure change in high-pressure nitrogen replacement of methane. *Energies* **2018**, *11*, 175.
(37) Chareonsuppanimit, P.; Mohammad, S. A.; Robinson, R. L., Jr.; Gasem, K. A. M. Modeling gas-adsorption-induced swelling and permeability changes in coals. *Int. J. Coal Geol.* **2014**, *121*, 98−109.

https://doi.org/10.1021/acsomega.1c02442
ACS Omega 2021, 6, 19115−19126